Alicyclic polyamide nanofilms with asymmetric structure for Cl^-/SO_4^{2-} separation

Bingbing Yuan[1], Shanshan Zhang[1], Chi Jiang[2,3], Ping Hu[1], Jiabao Cui[1], Siheng Zhao[1], Ning Wang[1], Q. Jason Niu[2,3]

1 School of Chemistry and Chemical Engineering, Key Laboratory of Green Chemical Media and Reactions, Ministry of Education, Henan Normal University, 453007 Xinxiang, Henan, China.

2 Institute for Advanced Study, Shenzhen University, 518060 Shenzhen, Guangdong, China.

3 State Key Laboratory of Heavy Oil Processing, College of Chemical Engineering, China University of Petroleum (East China), 266555 Qingdao, Shandong, China.

Email: yuanbingbing@htu.edu.cn and qjasonniu@szu.edu.cn

Abstract

Separation of mixed ion, especially Cl^- and SO_4^{2-}, is essential for reduced energy consumption and achievement of the minimal or zero-liquid discharge. Membrane technology has attracted significant attention in this respect owing to its good system coupling and maturity. However, it remains challenging to fabricate highly selective nanofilm with fine-tuning pore and structure that is suitable for the separation of Cl^- and SO_4^{2-}. Herein, we report an asymmetric alicyclic polyamide nanofilm with enhanced interconnectivity pore by manipulating the molecular geometry structure, composed of the porous aromatic polyamide dendrimer layer, and the dense alicyclic polyamide layer with hollow stripes. This resulted membrane shows a 107.14% separation rate of Cl^- and SO_4^{2-}, and a water flux (for Na_2SO_4) of ~2.2 times that of the pristine polyamide membrane. We estimate this fine-tuning pore approach resulting from alicyclic structure also might be employed in other separation membranes such as gas, solvent or neutral molecules.

KEYWORDS

Cl^-/SO_4^{2-} separation, alicyclic polyamide, asymmetric, contorted monomer

1 INTRODUCTION

Membrane technology, which is energy efficient and easy to modularize, provides an alternative to economically and environmentally resolve the problem of worldwide water scarcity and resource recycling.[1-4] For the industrial wastewater generated from the salt, chlor-alkali or coal chemical industry, wet smelting, pharmaceuticals and other industries, wastewater management strategy aimed at minimal or zero-liquid discharge (MLD/ZLD) are attracting heightened attention worldwide.[5] While membrane processes, such as water purification and desalination, have achieved substantial industrial success, the capability of state-of-the-art membranes to selectively separate a single solute or ion from a mixture of solutes is limited.[6] How to enhance the separation rate of Cl^- and SO_4^{2-} for the polyamide (PA) membrane used in MLD/ZLD process is one of the keys to reduce energy consumption and improve economic performance.[5] Otherwise, the lower separation rate of Cl^- and SO_4^{2-} could increase the number and stages of pressure vessels, and the burden on the followed evaporation crystallizer.[7] Thus, designing polyamide nanofiltration (NF) membrane with good separation rate or selectivity is of primary importance to achieve high energy efficiency in MLD/ZLD process.

Conventional polyamide nanofiltration (NF) membrane, has a composite structure, of which an active layer formed by interfacial polymerization (IP) through the trimesic acid chloride (TMC) and piperazine (PIP) on top of a porous support.[8] Based on the size exclusion and Donnan equilibrium effect in the separation process, this semi-aromatic polyamide (TMC-PIP) NF membrane exhibits the unsatisfactory separation rate of Cl^- and SO_4^{2-}.[9-11] Although extensive research work have been conducted to decrease the thickness of the polyamide nanofilm to increase the membrane permeance, most of the conventional IP process lacks to control the molecular-level design of the polyamide layer required for achieving high separation rate of ions for the specification composite membranes.[12] Efforts also have been applied to fine-tune the surface charge and porosity of the polyamide nanofilm to improve the membrane performance. Specifically, surface coating,[13-15] intermediate

layer,[16,17] alternatives amine or acid chloride monomers,[3,18,19] additives including surfactants,[12,20] macromolecules,[21,22] and nanoparticles,[23,24] have been adopted and successfully achieved the high selectivity and high performance. It has been found that there is a trade-off between water/salt or ion selectivity and pure water permeance.[25,26] And for membrane used in the separation of Cl^- and SO_4^{2-}, the good separation rate or selectivity is more important than that of high-water permeability in real application.[27] A compromised separation rate of Cl^- and SO_4^{2-} leads to an energy-intensive and complexed multi-stage process to achieve the retention of specific ions from a mixed salt feed.[7,28] Karan *et al.* produced TMC-PIP PA nanofilm with reduced pore sizes and narrow pore size distribution via the introduction of sodium lauryl sulfate (SLS) to kinetically control the cross-linking degree, and achieved a good separation performance between monovalent and divalent ions in high concentration mixed ions feed.[20] Zhu *et al.* incorporated the hydroxyl-terminated hyperbranched polyesters (HPEs) into the TMC-PIP PA nanofilm to construct a mixed matrix nanofilm with a modified pore structure and a more negatively charged surface, which exhibited a good separation rate between Cl^- and SO_4^{2-}.[29]

The above research demonstrates that, the separation of Cl^- and SO_4^{2-} for polyamide nanofilm is both closely related to its surface charge and the internal pore structure.[6,9,30] Additionally, previous work indicates that introducing the dendrimer porous layer onto the TMC-PIP PA nanofilm made by IP process enable to form the defect-free asymmetric PA nanofilm with hollow nanostrips structure. Nanofiltration performance was demonstrated for an enhanced permeance to the removal of salts from water, but unfortunately, these semi-aromatic polyamide membranes had no significant increase on the separation rate of Cl^- and SO_4^{2-}.[31]

Here we design and fabricate an asymmetric alicyclic polyamide nanofilm on molecular-level, which possesses enhanced microporosity and equivalent surface charge. It is known that the pore structure and distribution of polymer is essentially defined by the geometry of monomers.[32] We employed interfacial polymerization with contorted alicyclic acid chloride and amine monomers to synthesize defect-free,

crosslinked polyamide nanofilms with ~90 nm in thickness directly on dendrimer porous layer. The dendrimer porous layer enables the inconsonant diffusion-reaction of amine molecules, and obtain a stripe polyamide nanofilm. Moreover, the remained amine groups in the dendrimer porous layer can participate in the IP reaction, thereby forming an asymmetric polyamide nanofilm with a two-layer via stable covalent bonds. The nanofilms fabricated with two contorted monomers exhibit higher interconnectivity pore and larger mean effect pore size than those made from one contorted monomer, which is confirmed by our experimental results and molecular simulations. This results in a significant increase in the separation rate of Cl^- and SO_4^{2-} in the mixed ion solution compared with the commercial and conventional polyamide membranes (DK, XC-N, DL and NF 270). Moreover, the asymmetric alicyclic polyamide nanofilm exhibits a higher permeance owing to the formation of ordered nanovoids in the stripe and the decreased nanofilm thickness. This work demonstrates that the fine-tuning of pore and structure in nanofilm using both contorted monomers provide good separation rate between the mixed ions.

2 EXPERIMENTAL

2.1 Materials

Trimesoyl chloride (TMC), piperazine (PIP), trifluoroacetic anhydride, 3,5-diaminobenzoic acid, sodium nitrite, P-phenylenediamine and hydrazine hydrate were purchased from Tokyo Chemical Industry (Japan). Cyclopentane tetracarboxylic acid was obtained from Alfa Aesar. Sodium hydroxide, sodium chloride, magnesium chloride hexahydrate, anhydrous magnesium sulfate, sodium sulfate, calcium chloride, sodium hydrogen carbonate, N-Methyl-2-pyrrolidinone (NMP), thionyl chloride, tetrachloroethane, dichloromethane, ethyl acetate, acetonitrile, cyclohexane, n-hexane, hydrochloric acid, polyethylene glycol (PEG), methanol and N, N-Dimethylformamide (DMF) were obtained from Sinopharm Chemical Reagent Co., Ltd. and used without further treatment. Polysulfone (PSF) support were obtained from a commercial supplier (Origin Water). DK and DL were obtained from Suez Environnement. XC-N and NF 270 were obtained from DuPont. Deionized (DI) water

(0.5−1.5 μs/cm) was prepared in a two-stage reverse osmosis purification system. Coverslips with a thickness of 0.1−0.13 mm were purchased from Sail Brano Corp. and used as a support for scanning electron microscopy (SEM).

2.2 Preparation of cis, cis, cis, cis-1,2,3,4- cyclopentane tetracarboxylic acid chloride (CPTC)

The cyclopentane tetracarboxylic acid was dried under vacuum at 65°C and 1 mmHg for 15h. The dried cyclopentane tetracarboxylic acid (10.0 g, 0.04625 mol) was dispersed in chloroform (50 mL), distilled thionyl chloride (33.0 g, 0.2775 mol), and DMF (0.25 ml) at 80°C and refluxed for 3 h. The chloroform and excess thionyl chloride were removed under reduced pressure (1mm Hg) to obtain pure cyclopentane tetracarboxylic acid chloride (CPTC) product (80.7%, 11.9 g).

2.3 Preparation of asymmetric alicyclic polyamide membrane

G4 dendrimer was synthesized according to the previous report (Figure S3). The resulted G4 dendrimer was dissolved in the hydrochloric acid solution of pH=1 to form a 0.36 mM salt solution, and diazotization-coupling reaction was conducted on the PSF substrate under sodium nitrite solution (72.5 mM, pH=1) for 5 min at 0°C to form the dendrimer porous layer. The advantage of porous aromatic polyamide dendrimer layer is that this thin layer (50-60 nm) can overcome the aperture defect (inhomogeneity) of the underlying PSF support, and produces a more hydrophilic surface for IP required, to form the defect free nanofilms at the interface. Afterwards, an optimized interfacial polymerization formula was used to prepare alicyclic polyamide nanofilm, and the following are the detailed steps. The pristine PSF and PSF with dendrimer porous layer were firstly immersed into PIP solution (1.8 w/v%) for 2 min, respectively. Subsequently, the extra amine solution on the support surface was blown off with an air knife. Then, the above support was contacted with CPTC/n-hexane solution (0.1 w/v%) for 20s to form the conventional or asymmetric alicyclic polyamide nanofilm. And the organic phase solution on the surface was instantly blown off with an air knife. The resulted polyamide membranes were finally dried at

60°C for 2 min and stored in DI water until use. To demonstrate the role of asymmetric alicyclic polyamide nanofilm in the separation of Cl^-/SO_4^{2-}, the semi-aromatic polyamide (TMC-PIP) nanofilms were prepared as control membranes with the same formula and method. Moreover, four conventional and commercial semi-aromatic polyamide membranes (DK, XC-N, DL and NF 270) were also selected as control membranes to conduct the separation experiments and further illustrated the potential advantage of asymmetric alicyclic polyamide membrane on the separation of Cl^-/SO_4^{2-}.

2.4 Characterization

Nuclear magnetic resonance (NMR) spectroscopy (BRUKER, Germany) was conducted to verify the purity of the prepared CPTC monomer. Approximately 5−15 mg product was loaded into the NMR tube and dissolved with 2−3 mL $CDCl_3$ for ^1H NMR and ^{13}C NMR characterization. The data were analyzed with MestReNova software. The chemical composition and structure of the CPTC-PIP, asymmetric CPTC-PIP (A-CPTC-PIP) and TMC-PIP were characterized by attenuated total reflectance fourier transform infrared spectroscopy (ATR-FTIR) and X-ray photoelectron spectroscopy (XPS), respectively. The chemical composition and elemental data obtained from XPS were analyzed and fitted using CasaXPS software. Surface charge of the CPTC-PIP, asymmetric CPTC-PIP (A-CPTC-PIP) and TMC-PIP membranes were determined with an Anton Paar SurPass solid surface analyzer. And water contact angle was measured under room temperature (25°C) using a drop shape Analyzer-DSA30 (KRÜSS, Germany) in the sessile drop mode for characterizing the surface hydrophilicity of the membrane surface. Densities of polyamide dendrimer porous layer, A-CPTC-PIP, CPTC-PIP, and TMC-PIP PA layers were measured and calculated by the ellipsometry (J. A. Woollam Co., Lincoln, NE) and QCM (Q-Sense, Explorer, Biolin Scientific). As shown in Figures S5 and S6, it should be noted that we used the polyamide dendrimer porous layers in that the diazotization coupling reaction processes were conducted 2 or 4 times as samples to analyze their volumetric mass densities. The polyamide layers that need density

measurement were separated from the PSF support, and deposited onto the QCM sensors. Using the method previously reported,[31] we conducted the scanning electron microscopy observation (SEM, Hitachi SU8010) characterizations to analyze the surface and cross-sectional morphology of the prepared polyamide nanofilms. It should be noted that the internal and external morphologies of the prepared polyamide nanofilms were investigated by transmission electron microscope (TEM, JEM-1200EX, JEOL). Here, the inner surface of the polyamide nanofilm refers to the surface contacting the PSF support, and the outer surface refers to the surface of the polyamide layer formed after interfacial polymerization.

2.5 Separation performance evaluation

The separation performance of the resulted polyamide membranes was determined with single or mixed salt solutions in a cross-flow system, with an effective test area (A) of 28.12 cm^2. The separation performance tests were conducted at an operating pressure of 1 MPa and a temperature of 25°C. The performance data were determined after the water flux and conductivity reached a steady state. For the membrane stability test, the asymmetric alicyclic polyamide membrane was operated continuously for 4-6 hours a day at 1 MPa and 25°C in a period of 20 days to measure the changes in its Cl^-/SO_4^{2-} separation rate and water flux. Among them, the concentrations of Cl^- and SO_4^{2-} in the mixed salt solution were tested by an ion chromatograph system (Thermo Dionex Aquion).

The water flux (kg m^{-2} h^{-1}) was calculated from the weight of the permeation (M) for a specified time, as given by the following equation:

$$\text{Water Flux (kg m}^{-2}\text{ h}^{-1}\text{)} = M/At \qquad (1)$$

The salt (ion) rejection was determined from the conductivity (ion concentration) of the feed solution (C_f) and the permeation (C_p). Hence, the salt (ion) rejection can be calculated from the following equation:

$$\text{Rejection (\%)} = \left(1 - C_p/C_f\right) \times 100\% \qquad (2)$$

The separation rate of Cl^- and SO_4^{2-} in the mixed salt solution is defined as

follows:

$$\text{Separation rate (\%)} = R_{SO_4^{2-}}(\%) - R_{Cl^-}(\%) \quad (3)$$

The separation selectivity of Cl^- and SO_4^{2-} in the mixed salt solution for the asymmetric CPTC-PIP and commercial polyamide membranes (XC-N, DK, DL, NF270) can be calculated by the followed equations:

$$S_{Cl^-/SO_4^{2-}} = \frac{100 - R_{Cl^-}(\%)}{100 - R_{SO_4^{2-}}(\%)} \quad (4)$$

The variation of molecular weight cut-off (MWCO) and mean effective pore size for the asymmetric CPTC-PIP and TMC-PIP polyamide membrane, were characterized by the solute transport method. Polyethylene glycol (PEG 200, 400, 600, 800 and 1000) of 0.2 g L^{-1} were used to measure the molecular weight cut-off (MWCO) and solution rejection (R_T) of the resulted membrane. The solution rejection (R_T) can be obtained according to the following equation:

$$R_T = \left(1 - \frac{C_p}{C_f}\right) \times 100\% \quad (5)$$

Where C_p is the total organic carbon (TOC) of permeation solution, C_f is the TOC of feed solution.

The relationship between Stokes radius r_s and molecular weight, M_W, of these PEGs solutes can be expressed by the following equation:

$$r_s(\text{nm}) = 16.74 \times 10^{-3} \times Mw^{0.557} \quad (6)$$

Where r_s is nm and M_W is g mol^{-1}, respectively. From this equation, the radius of a hypothetical solute at a given M_W can be obtained. The MWCO, which refers to as the molecular weight that above 90% of the solute in the feed solution is retained by the membrane.

By plotting the solute rejection against the PEG Stokes diameter in a log-normal probability plot, a straight line and a linear equation would be obtained through curve fitting. From this equation, the mean solute size (μ_s) could be obtained when R_T was

50%, and σ_g (geometric standard deviation of μ_s) was determined from the ratio of d_s at R_T= 84.13% and 50%. By ignoring the steric and hydrodynamic interaction between the solute and the pore size, the mean pore size (μ_p) and the geometric standard deviation (σ_p) were the same as μ_s and σ_g, respectively.

3 RESULTS AND DISCUSSION

3.1 Fabrication of the asymmetric alicyclic polyamide nanofilm

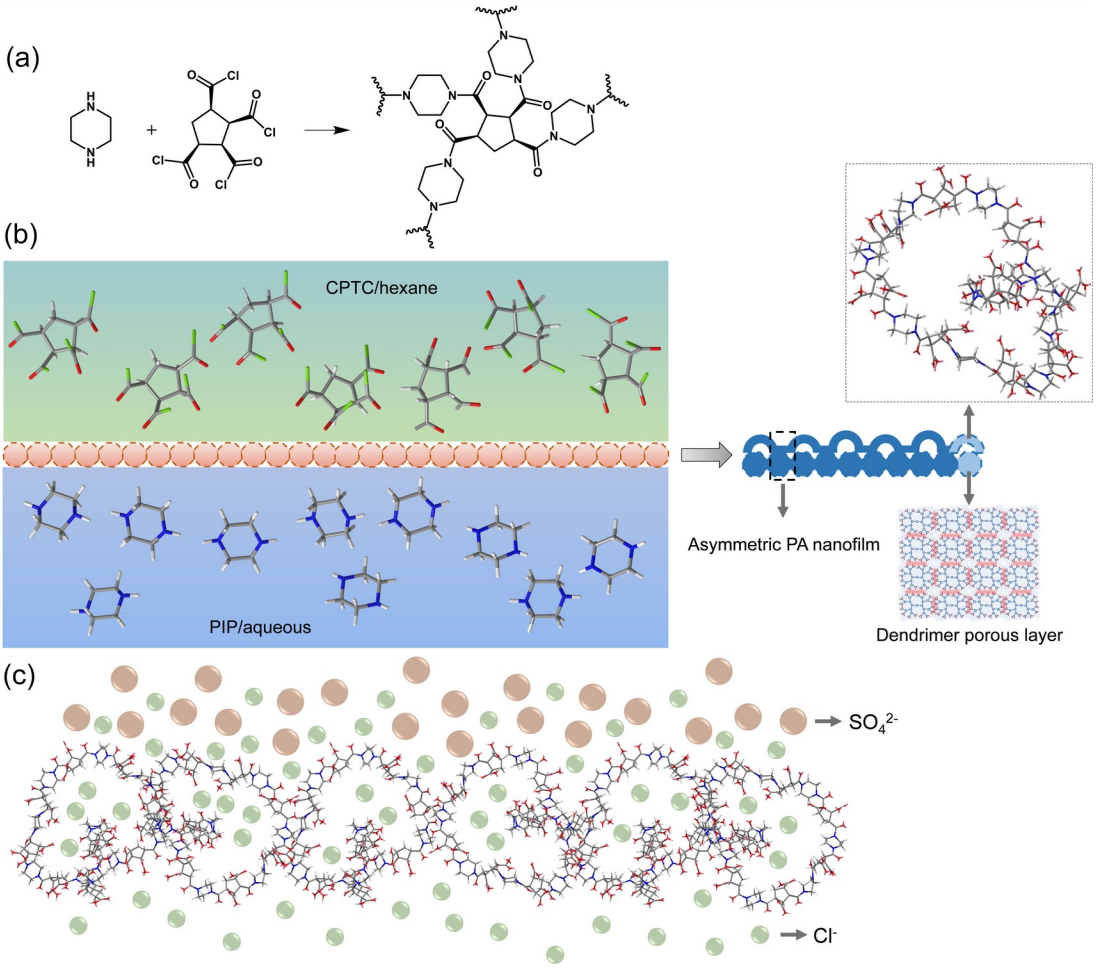

FIGURE 1 (a) Synthesis of alicyclic polyamide nanofilms through interfacial polymerization. (b) Visualization of the interfacial polymerization between CPTC in hexane and the PIP in aqueous solution. And the asymmetric polyamide nanofilm composed of dendrimer porous layer and CPTC-PIP polymer segments. (c) Schematic diagram of an alicyclic polyamide nanofilm for Cl^-/SO_4^{2-} sieving.

The conventional acid chlorides monomer used in IP is non-distorted, and co-planar

aromatic acid chloride, such as TMC, as shown in Figure S4. The alicyclic acid chlorides monomer is a class of distorted and non-coplanar structure, which can be utilized in the IP process to enhance the interconnectivity of intermolecular voids of PA network (as illustrated in Figure S4). The CPTC monomer with distorted and non-coplanar structure was thus selected and synthesized to fabricate the alicyclic polyamide nanofilm. Previous work indicated that introducing dendrimer porous layer into IP process enabled to form a stripe polyamide nanofilm containing ordered nanovoids, and produced an asymmetric polyamide nanofilm with a two-layer nanostructure, namely dendrimer porous layer and polyamide dense layer, with crosslinking each other. Here, alicyclic polyamide nanofilms with asymmetric structure were formed by reacting a PIP with CPTC at the interface between two immiscible solutions (Figures 1a and 1b). We selected TMC with planar structures as non-contorted controls. As demonstrated in Figure S4, the acid chloride bond and

cyclopentane within CPTC has an angle of more than 90°, so when it reacts with PIP,

the CPTC units are held in non-coplanar orientation by the polymer network, enhancing interconnectivity of network voids (Figure 1b). The distorted conformation prohibits the efficient packing of polymer segments in the networks, leading to relatively higher free volume. Figure 1c shows the schematic diagram that the alicyclic polyamide nanofilm with enhanced porosity used as selective layer for the separation of Cl^- and SO_4^{2-}.

3.2 Membrane morphologies and microstructures

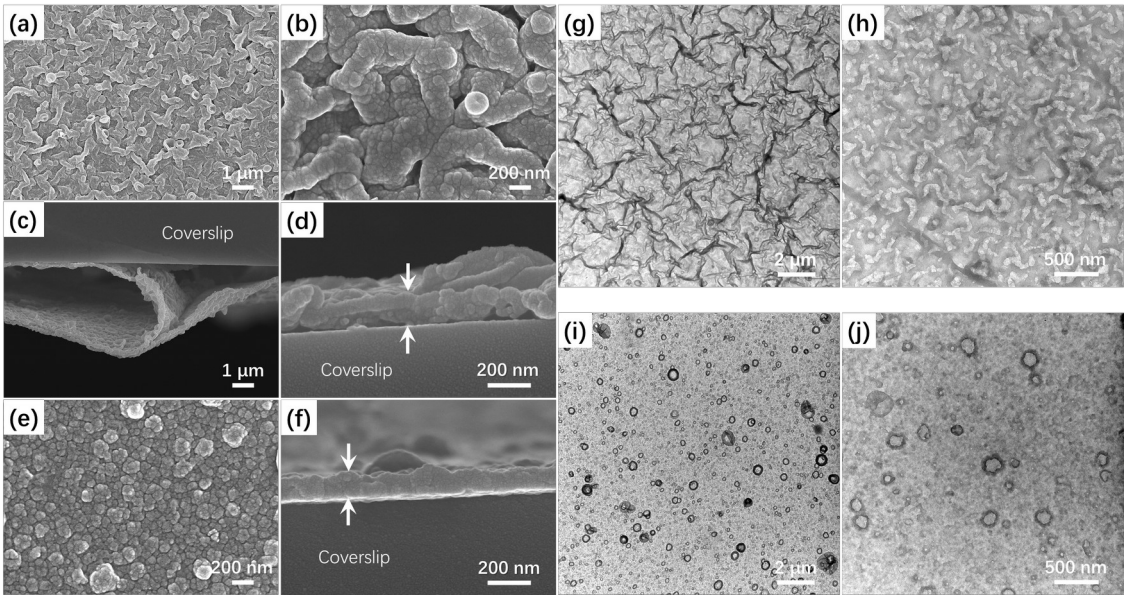

FIGURE 2 (a b) Low and high-magnification SEM images of the asymmetric CPTC-PIP PA nanofilm surfaces. (c d) Low and high cross-sectional SEM images of the asymmetric CPTC-PIP PA nanofilms. (e) High-magnification SEM images of the CPTC-PIP PA nanofilm surfaces. (f) High cross-sectional SEM images of the CPTC-PIP PA nanofilm. (g and h) Outer and inner surface TEM images of the asymmetric CPTC-PIP PA nanofilms. (i and j) Outer and inner surface TEM images of the CPTC-PIP PA nanofilms.

To investigate the inner and cross-sectional morphology of the resulted IP polyamide nanofilm, we conducted the SEM and TEM measurements (Figures S10–S17). The asymmetric alicyclic polyamide nanofilms with stripe can be formed through interfacial polymerization on the dendrimer porous layer (Figures S5 and S6), as shown in Figures 2a and 2b. High-magnification SEM images in Figure 2b shows that the width of stripe is ~200 nm. Asymmetric alicyclic polyamide nanofilms with thickness ~140 nm formed through IP, were transferred onto coverslip supports, allowing clear imaging with SEM (Figures 2c and 2d). It is noted that, it is the Figure 2c and Figure S11 that exhibit the overlapped morphology of the two asymmetric alicyclic PA layers. Figure 2d demonstrates that the alicyclic asymmetric polyamide nanofilm has a two-layer structure, of which the lower is a dendrimer porous layer with thickness 50-60 nm, and the upper is a nano-stripe polyamide dense layer with

thickness ~90 nm.

On the other hand, the conventional CPTC-PIP PA nanofilms in Figure 2e shows a nodule structure with a diameter ranged from 70 to 200 nm. High cross-sectional SEM images of the CPTC-PIP PA nanofilm exhibits a thickness of ~105 nm, without significant strip structure. Moreover, outer surface TEM images of the asymmetric CPTC-PIP polyamide nanofilm in Figure 2g and Figure S13 clearly found that the there is a hollow structure inside the nano-stripe (Figure S13d). Further inner surface TEM images in Figures 2h and S14 of the asymmetric CPTC-PIP PA nanofilms reveals that nano-stripes exhibit a uniform and ordered nanovoids structure inside, a width of 70 to 120 nm. For the conventional CPTC-PIP PA nanofilms in the Figures 2i and 2j, Figures S15 and S16, the outer and inner surface TEM images show that the nanovoids just marginally exist in the nodule structure, with a width of 50 to 200 nm.

These characterizations clearly indicate that, the asymmetric alicyclic polyamide nanofilm having a two-layer structure exhibits a dendrimer porous layer and an inner uniform, nanovoids polyamide denser layer. Hence, compared with the conventional CPTC-PIP polyamide nanofilm, the asymmetric alicyclic polyamide nanofilm is effective to reduce the transmembrane resistance of water and significantly increase the permeation flux.

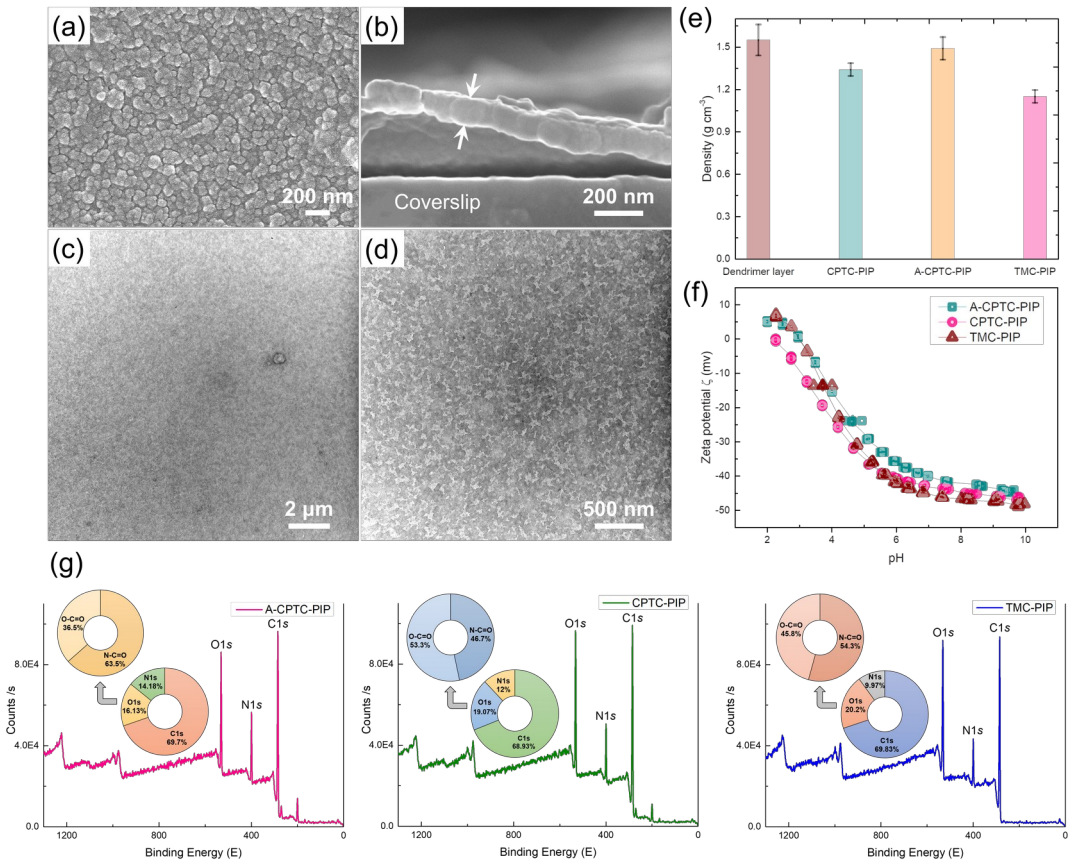

FIGURE 3 (a) High-magnification SEM images of the TMC-PIP PA nanofilm surfaces. (b) High cross-sectional SEM images of the TMC-PIP PA nanofilm. (c d) Low and high cross-sectional SEM images of the asymmetric CPTC-PIP PA nanofilms. (c d) External and internal surface TEM images of the TMC-PIP PA nanofilms. (e) Volumetric mass densities calculated for the dendrimer porous layer, and the polyamide active layers of the three membranes studied using the areal masses obtained from QCM analyses and thicknesses from ellipsometry analyses. (f) Representative ζ potential of the fabricated conventional and asymmetric polyamide nanofilms. The membrane zeta potentials were estimated by measuring the ζ potentials in a background electrolyte solution of 1 mM KCl. All measurements were performed at 25°C and repeated 4 times. (g) XPS spectra, the corresponding elemental compositions (insets) of the asymmetric CPTC-PIP (A-CPTC-PIP), CPTC-PIP and TMC-PIP PA nanofilms. And the corresponding plausible species determined from the deconvolution of O1*s* core level XPS spectra.

Besides, as non-contorted structure controls, we used the conventional TMC

monomer with planar structure to react with PIP through IP on the pristine PSF supports, and fabricate the semi-aromatic polyamide nanofilms. High-magnification SEM images of the TMC-PIP PA nanofilm surfaces in Figure 3a exhibits a nodule structure, which is similar with the conventional CPTC-PIP PA nanofilm. The thickness of the TMC-PIP PA nanofilm shown in Figure 3b is ~100 nm, and also were transferred on coverslip support for clear observation. External and internal surface TEM images of the TMC-PIP PA nanofilms (Figures 3c, 3d, and Figures S19, S20) demonstrate that there are nodules on the external surface and inconspicuous nanovoids on the inner surface.

Furthermore, as shown in Figure 3e, we investigated the volumetric mass densities of the dendrimer porous layer, conventional CPTC-PIP, asymmetric CPTC-PIP and TMC-PIP nanofilms, and the results are 1.55± 0.11 g cm^{-3}, 1.34± 0.05 g cm^{-3}, 1.49± 0.08 g cm^{-3}, 1.15± 0.05 g cm^{-3}, respectively. It was found that the density value of the asymmetric CPTC-PIP nanofilms is located between the dendrimer porous layer and the CPTC-PIP polyamide nanofilm. The density features thus confirm the formation of the asymmetric alicyclic polyamide nanofilms comprised two layers.

In addition, after the IP reaction, unreacted carboxyl and amine groups can be ionized, depending on the pH of the solution in contact with the polyamide nanofilm.[33] The isoelectric point (IEP, the point of zero charge, i.e., the pH at which the number of ionized amine groups is equal to the number of ionized carboxyl groups) of the asymmetric CPTC-PIP polyamide nanofilm is slightly higher than that of the conventional CPTC-PIP polyamide nanofilm, and the surface zeta potential value of the former is thus less negative than that of the latter.[34,35] For example, the related zeta potential value at pH=7 is -45.3 mV for TMC-PIP nanofilm, -43.3 mV for CPTC-PIP nanofilm, and -40.2 mv for asymmetric CPTC-PIP nanofilm, respectively. From the XPS results (Figure 3g, Figure S9, and Table S1), the lower −COOH content in the asymmetric alicyclic polyamide nanofilm is mainly responsible for the slightly decreased surface negative charge. Besides, considering a lower O/N ratio, the asymmetric CPTC-PIP PA nanofilm thus exhibits a higher degree of network cross-

linking than that of the conventional CPTC-PIP PA nanofilm. These characterizations illustrate that the dendrimer porous layer can affect the composition structure and the morphology of the resulted polyamide nanofilm. And an equivalent negative surface charge was formed on the asymmetric alicyclic polyamide nanofilm, which produced the Donnan effect on the ions that permeate through the membranes.

3.3 Separation performance

TABLE 1 Separation performance of the asymmetric CPTC-PIP, CPTC-PIP and TMC-PIP polyamide membranes, reaction time: 20s. The operating pressure and temperature were controlled at 1 MPa, 25°C. The feed flow rate was 7.5 L min^{-1}, and the salt concentrations in the feed solutions were 2000 ppm.

	Asymmetric CPTC-PIP		CPTC-PIP		TMC-PIP	
Salt	Rejection (%)	Water flux (kg m^{-2} h^{-1})	Rejection (%)	Water flux (kg m^{-2} h^{-1})	Rejection (%)	Water flux (kg m^{-2} h^{-1})
Na_2SO_4	98.9±0.2	133.4±3.6	97.5±0.3	60.8±2.97	98.9±0.4	62.6±1.9
NaCl	13.6±3.4	146.5±4.5	12.4±1.3	81.1±4.49	46.5±1.94	64±2.26
$MgSO_4$	98.2±0.3	127.6±2.4	96.2±0.2	57.7±3.4	98.3±0.5	60.3±3.37
$CaCl_2$	44.7±4.3	138.3±5.7	46.5±1.8	64.2±4.4	63.8±2.28	64.9±0.42
$MgCl_2$	62.4±3.7	139.2±4.3	60.9±2.1	66.4±3.4	80.23 ± 2.1	61.87±2.9

As shown in Table 1, we measured the separation performance for single salt solution of the fabricated TMC-PIP, CPTC-PIP and asymmetric CPTC-PIP PA nanofiltration membranes, and further explored the relationship between structure and separation performance. Performance tests were conducted ~1 hour after starting the filtration to stabilize the rejection rate and water flux. The calculated data demonstrate that, the asymmetric alicyclic CPTC-PIP PA membrane has an enhancement in water flux and rejection compared to the CPTC-PIP membranes. For the CPTC-PIP PA membrane, Na_2SO_4 rejection rate of the asymmetric alicyclic polyamide membrane increases from 97.5% to 98.9%, and the corresponding water flux increases from 60.8 kg m^{-2} h^{-1} to 133.4 kg m^{-2} h^{-1}. Based on the SEM and TEM analyses, the enhancement in water flux is mainly attributed to the formation of the nano-stripes with ordered nanovoids structure, and the decreased thickness in the polyamide dense layer. Generally, the uniform, ordered hollow nano-stripes inside can increase the water permeable area of

unit nanofilm area, and improve the water transmission efficiency. According to the solution-diffusion model and corresponding water flux equation (Equation S1), the thinner polyamide dense layer enables to lower the resistance of water transport across the active layer, and thereby improve permeance. Moreover, it is found that the asymmetric alicyclic CPTC-PIP membrane exhibits the highest separation rate of Na_2SO_4 and NaCl among the three PA nanofiltration membranes. Specifically, the separation rate of Na_2SO_4 and NaCl for asymmetric CPTC-PIP PA membrane is 85.3%, while that for conventional TMC-PIP membrane is 52.4%. More importantly, as demonstrated in Table S3, compared with the commercial polyamide nanofiltration membranes, such as DK, XC-N, DL and NF270, the asymmetric CPTC-PIP PA still shows the highest separation rate of Na_2SO_4 and NaCl.

3.4 Comparation of Cl^-/SO_4^{2-} separation rate

TABLE 2 Cl^-/SO_4^{2-} separation performance of the asymmetric CPTC-PIP, commercial DK, XC-N, DL, and NF270 membranes.

Membrane	Salt mixture solution	Ion rejection rate (%)		Separation rate of Cl^- and SO_4^{2-} (%)	$S_{Cl^-/SO_4^{2-}}$
		Cl^-	SO_4^{2-}		
Asymmetric CPTC-PIP	Feed 1a	15.5	98.9	83.4	76.8
	Feed 2a	-8.24	98.9	107.14	98.4
DK	Feed 1a	46.6	98.5	51.9	35.6
	Feed 2a	21.3	98.8	77.5	65.6
XC-N	Feed 1a	51.4	98.6	47.2	34.7
	Feed 2a	24.7	98.7	74.0	57.9
DL	Feed 1a	47.95	98.6	50.7	37.2
	Feed 2a	20.54	98.9	78.4	72.2
NF270	Feed 1a	50.84	98.7	47.9	37.8
	Feed 2a	23.63	98.9	75.3	69.4

a Feed solution was composed of 1.0 g L^{-1} NaCl and 1.0 g L^{-1} Na_2SO_4.

b Feed solution was composed of 2.0 g L^{-1} NaCl and 2.0 g L^{-1} Na_2SO_4.

In order to evaluate the separation rate of the SO_4^{2-} and Cl^- of the asymmetric CPTC-PIP polyamide membrane, we used the NaCl/Na_2SO_4 binary salt mixture solution as the feed solution, and compared with four kinds of commercial NF membranes made

by TMC-PIP. DK, XC-N, DL and NF270 are the common semi-aromatic polyamide nanofiltration membranes, which are widely used in various of industrial water treatment processes such as selective ion screening. As shown in Table 2, it is well known that Cl^- possesses a lower valence and smaller size than that of the SO_4^{2-}, based on size exclusion and Donnan equilibrium, the Cl^- is thus forced to permeate preferentially through the PA nanofilm. In addition, the negatively charged PA nanofilm surface can further imparts an increase in the SO_4^{2-} rejection rate, as illustrated in the Figure 3f. Generally, for the PA NF membranes, the SO_4^{2-} rejection rate is higher than that of Cl^-. The Cl^- rejection of asymmetric CPTC-PIP membrane is lower than that of the commercial PA membranes, such as DK, XC-N, DL and NF270, which is mainly attributed to interconnectivity of network voids. For example, under the mixed feed solution of 2 g L^{-1} NaCl and 2.0 g L^{-1} Na_2SO_4, separation rate of Cl^- and SO_4^{2-} for the asymmetric CPTC-PIP PA membrane is 107.14%, and the corresponding selectivity of Cl^- and SO_4^{2-} is 98.4, which is the highest among the five kinds of PA NF membranes. These results demonstrates that the alicyclic polyamide membrane with asymmetric structure shows an advantage on the separation of Cl^- and SO_4^{2-} compared with the conventional and commercial semi-aromatic PA (TMC-PIP) membranes.

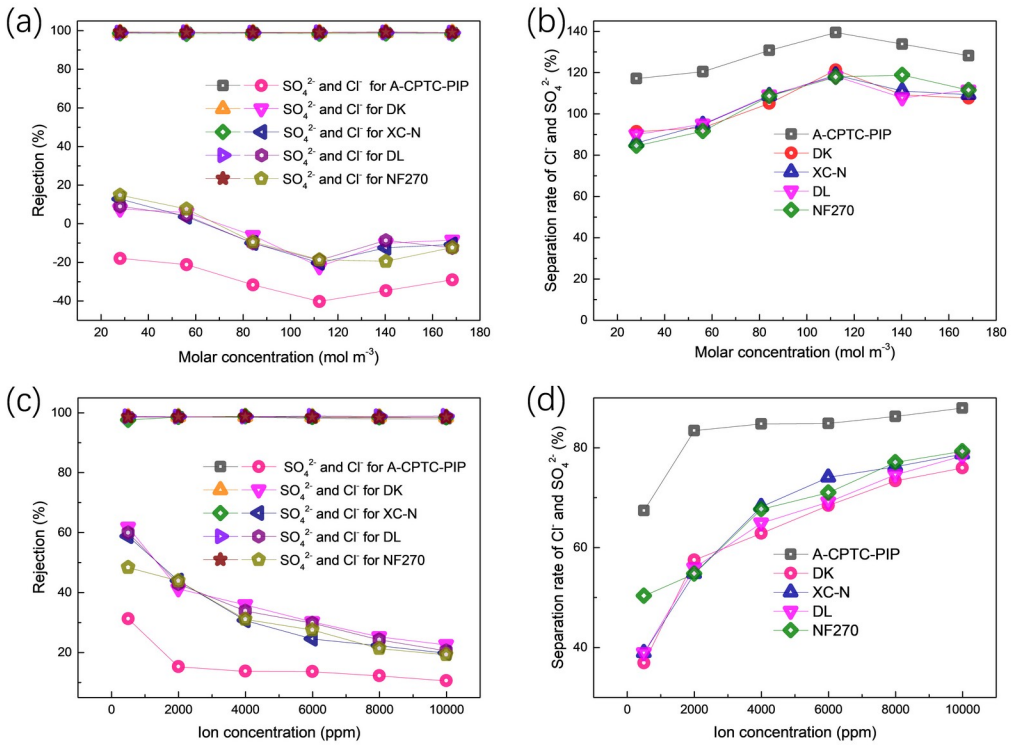

FIGURE 4 Cl^-/SO_4^{2-} separation performance of the asymmetric CPTC-PIP (A-CPTC-PIP), commercial DK, XC-N, DL and NF270 membranes. (a b) Effect of the mixed solution of Cl^- and SO_4^{2-} with different content of equimolar concentration on the separation performance of Cl^-/SO_4^{2-}, (c d) Effect of the single ion concentration of Cl^- and SO_4^{2-} on the separation performance of Cl^-/SO_4^{2-}.

In actual industrial applications, concentrated salt solutions containing NaCl and Na_2SO_4 usually present a higher concentration, up to 100 mol m^{-3}, so it is necessary to conduct a salt separation test under this feed solution condition. We used the Cl^-/SO_4^{2-} binary mixture anion solution with equimolar concentration as the feed solution, to investigate the asymmetric alicyclic CPTC-PIP PA membrane and the other four commercial semi-aromatic PA membranes for the separation performance of Cl^- and SO_4^{2-}. As shown in Figures 4a and 4b, it is found that both semi-aromatic polyamide and alicyclic polyamide nanofiltration membranes show a high rejection (>99%) for SO_4^{2-} and a negative rejection rate for Cl^- when the molar concentration varied in the range of 28.08 to 168.48 mol m^{-3}. However, the alicyclic CPTC-PIP polyamide membrane exhibits a significantly lower Cl^- rejection than that of the commercial

semi-aromatic membranes such as DK, XC-N, DL and NF270. Under 112.32 mol m^{-3} mixed anion solution, the asymmetric alicyclic CPTC-PIP polyamide membrane gives a -40.41% rejection for the Cl^-, whereas the commercial DK membrane exhibits a -22.38% Cl^- rejection. And the corresponding separation rate of Cl^- and SO_4^{2-} for the A-CPTC-PIP and DK membranes are 134.41%, 121.28%, respectively.

Moreover, we also evaluated the effect of the single anion concentration (Cl^- or SO_4^{2-}) varied in the range of 500 to 10,000 ppm on the separation performance of Cl^-/SO_4^{2-}. As illustrated by Figures 4c and 4d, the alicyclic CPTC-PIP PA membrane exhibits a lower Cl^- rejection than that of the commercial NF membranes, which is in the range of 31.52% to 10.52%. It is worthy noted that two chemical structures reveal no significant differences on the divalent ion rejection, but the alicyclic PA structure has the ultralow monovalent anion retention. The alicyclic CPTC-PIP polyamide structure thus enables to show an efficient screening between Cl^- and SO_4^{2-}, and the corresponding separation rate of Cl^- and SO_4^{2-} is in the range of 67.4% to 88.0% (Figures 4c and 4d). These results further illustrate that the alicyclic CPTC-PIP PA membrane is more suitable for separating mixed salt solutions containing Cl^- and SO_4^{2-}, compared with the conventional semi-aromatic PA membranes such as commercial DK, XC-N, DL and NF270.

3.5 Effect of Ca^{2+} and Mg^{2+} on separation rate

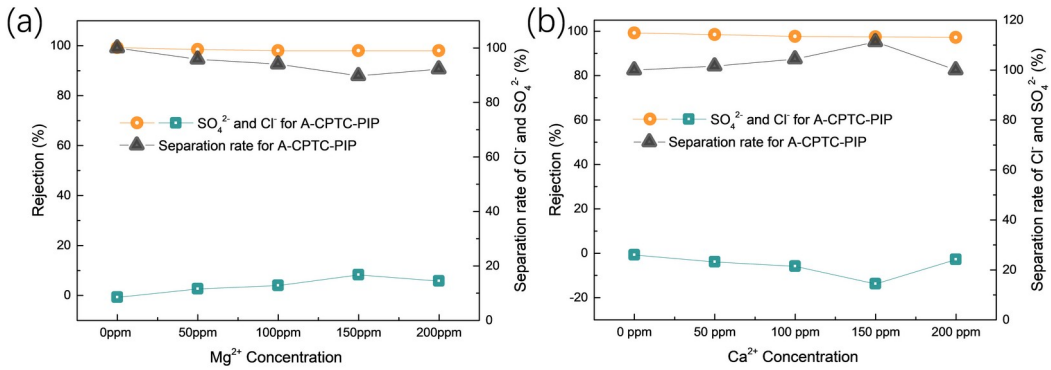

FIGURE 5 Cl^-/SO_4^{2-} separation performance of the asymmetric CPTC-PIP PA membranes. (a) Effect of the Mg^{2+} concentration on the separation performance of Cl^-/

SO_4^{2-}, (b) Effect of the Ca^{2+} concentration on the separation performance of Cl^-/SO_4^{2-}. Feed solution: 1000 ppm Cl^- and 1000 ppm SO_4^{2-} mixed solutions.

In the MLD/ZLD processes, the feed solution generally contains a small amount of Ca^{2+} and Mg^{2+}, we thus investigated the effect of the Mg^{2+} and Ca^{2+} concentration on the separation performance of Cl^-/SO_4^{2-}. As shown in Figures 5a and 5b, with the addition of Mg^{2+} and Ca^{2+}, the corresponding Cl^- rejection rate for the alicyclic CPTC-PIP PA membrane have shown a slight increase. For example, the Cl^- rejection increases from -6.05% to 9.01% when the Mg^{2+} varied from 0 ppm to 200 ppm, while the SO_4^{2-} rejection is approximately constant (99.21% to 98%). Then the separation rate of Cl^- and SO_4^{2-} is successively decreased from 105.71% to 90.37%. Hence, Ca^{2+} and Mg^{2+} in the Cl^-/SO_4^{2-} binary mixture anion solution can reduce the separation rate of Cl^- and SO_4^{2-}. This enhancement in Cl^- rejection rate can be explained that, based on the Donnan equilibrium, the introduction of cations with high valence such as Ca^{2+} and Mg^{2+} suppress the permeation of Cl^- through the polyamide membranes with surface negative charge. In the case of anions, SO_4^{2-} with a valence of -2 will experience greater electronegative repulsion from the negatively charged membrane surface as opposed to Cl^-. The introduction of Ca^{2+} and Mg^{2+} effects the surface negative charge, resulting in a decrease on the Donnan exclusion when the SO_4^{2-} transports the PA nanofilm. The separation rate of Cl^- and SO_4^{2-} thus is slightly decreased.

3.6 Membrane stability

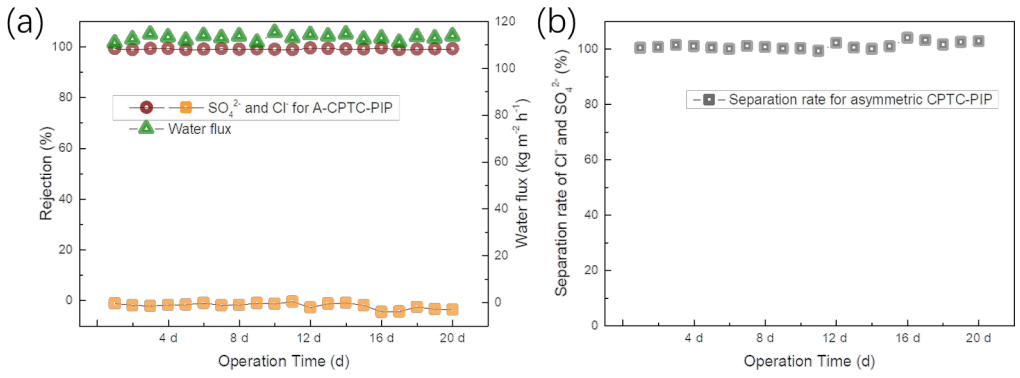

FIGURE 6 Operational stability. (a b) Operational stability of the asymmetric CPTC-PIP polyamide membrane. (c) Rejection curves to PEG with different molecular weight and the mean effective pore size (r_p) of the TMC-PIP and asymmetric CPTC-PIP PA membranes. (d) Simulated cavity size distributions in the CPTC-PIP and TMC-PIP polymers.

Operational stability is one of the key properties for the alicyclic asymmetric polyamide membrane used in terms of the separation of Cl^- and SO_4^{2-}, we thus conducted the long-term stability test (Figure 6). The experiment reveals that the asymmetric polyamide membrane exhibits a good operational stability during 20 d cross-flow test under 1 MPa for $NaCl/Na_2SO_4$ binary salt mixture solution containing 1000 ppm SO_4^{2-} and 1000 ppm Cl^-, of which the separation rate of Cl^- and SO_4^{2-} remains at between 99.2 % and 103.9% and water flux ranges from 110.6 kg m^{-2} h^{-1} to 115.1 kg m^{-2} h^{-1}. During the 20-day stability test, the asymmetric alicyclic polyamide membrane (CPTC-PIP) still showed a higher separation rate of Cl^- and SO_4^{2-} than that of the commercial semi-aromatic polyamide membranes (DK, XC-N, DK and NF270), as shown in Table S5.

3.7 Pore size distributions

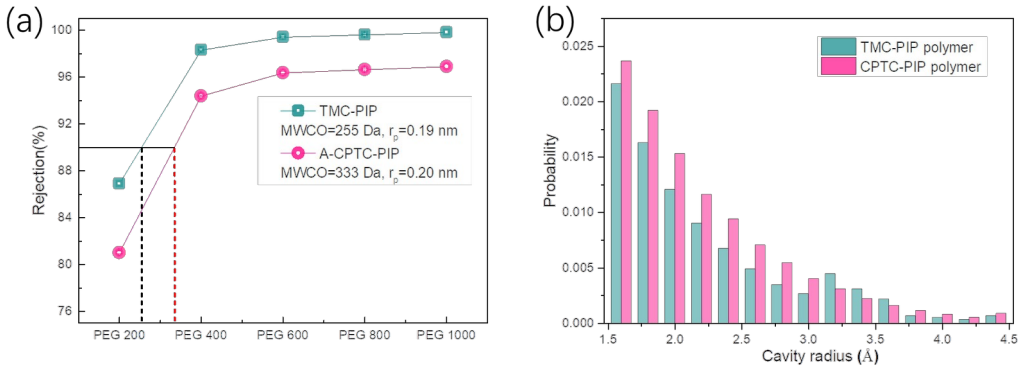

FIGURE 7 Pore size distributions. (a) Rejection curves to PEG with different molecular weight and the mean effective pore size (r_p) of the TMC-PIP and asymmetric CPTC-PIP PA membranes. (b) Simulated cavity size distributions in the CPTC-PIP and TMC-PIP polymers.

Synthetic membranes with pores at the sub-nanometer scale is imperative for the separation ion from a mixture of solutes.[30] On the basis of the solute transport method, [39] we estimated the molecular weight cut-off (MWCO) and mean effective pore size of the alicyclic and semi-aromatic polyamide nanofilms. As shown in Figure 7a, the MWCOs for the asymmetric CPTC-PIP (A-CPTC-PIP) and TMC-PIP polyamide membranes are 333 Da, 255 Da, respectively. The calculated mean effective pore radius for the A-CPTC-PIP membrane (0.20 nm) is higher than that of the conventional TMC-PIP membrane (0.19 nm). Besides, to further investigate the sub-nanometer pores distribution inside the alicyclic and semi-aromatic polyamide nanofilm, we performed the molecular simulations proposed by Bhattacharya and Gubbins.[36] Pore sizes were estimated by probing local free space using a particle with a specified radius size and the probe size was set at 1.6 Å. As shown in Figure 7b, the alicyclic polyamide shows mostly interconnected voids than that of the semi-aromatic polyamide, confirming that distorted, un-coplanar monomer resulted in an enhanced porosity. The structural analyses of the semi-aromatic polyamide and alicyclic polyamide models (Figure S25) show interconnected and disconnected voids with respect to a probe with a radius of 1.95 Å, of which, CPTC-PIP shows more interconnected voids (grey color) than that of the TMC-PIP.[37] This is consistent with comparable single salt and mixed ion experimental results (Tables 1 and 2, Figures 4 and 5). Specifically, the alicyclic polyamide presents an enhanced probability in the range of 1.95 Å and 3.0 Å compared with that of the semi-aromatic polyamide, counted as permeable area for Cl^- (1.95 Å for hydrated radius, Table S4), which is responsible for the lower Cl^- rejection.[38] For SO_4^{2-} with a hydrated radius of 3.0 Å, according to size exclusion and Donnan equilibrium, both alicyclic and semi-aromatic polyamides exhibit high rejection rates. These results indicate that the asymmetric alicyclic polyamide nanofilm exhibits an enhanced efficient size exclusion effect on the Cl^- to be separated, and thus a high separation rate for Cl^- and SO_4^{2-} can be achieved.

4 CONCLUSIONS

In summary, the alicyclic polyamide nanofilm with asymmetric structure was successfully formed on the PSF support via the IP process, of which the lower was a dendrimer porous layer, and the upper was the dense alicyclic polyamide layer with the nano-striped structure containing ordered nanovoids. The asymmetric alicyclic polyamide membrane exhibits good separation performance of Cl^- and SO_4^{2-}, whether in single or mixed salt solutions, where they are both more permeable and more selective than the commercially available polyamide membranes such as DK, XC-N, DL and NF 270. The enhancement in water flux is mainly attributed to the formation of the uniform, ordered hollow nano-stripes and the slightly decreased thickness of the alicyclic polyamide nanofilm. And the increased interconnected voids in the range of 1.95 Å and 3.0 Å and the negative surface charge are responsible for the increase in the separation rate of Cl^- and SO_4^{2-} for the asymmetric alicyclic polyamide nanofilm. Thus, this work might inspire the molecular design on the porosity tuned of polyamide nanofilm using the monomer with distorted conformation, to apply in the terms of molecule, gas separation. Moreover, adopting the asymmetrical concept to design the nanofilm structure is one of the effective means to improve the separation membrane performance, with great potential for applications in molecular separations, including organic solvent nanofiltration, seawater desalination, water purification and pervaporation, etc.

ACKNOWLEDGMENTS

This work was financially supported by the National Natural Science Foundation of China (Grant No. 22008056, U2006230), the Fund for Key Scientific and Technological Projects of Henan Province (Grant No. 202102210226), Key scientific research projects of colleges and universities in Henan Province (Grant No. 21A430021), the Shandong Province Major Science and Technology Innovation Project (Grant No. 2018CXGC1002). We would like to thank Y.W. Qin, Y.X. Hu and State Key Laboratory of Separation Membranes and Membrane Processes for QCM and ellipsometry analyses.

REFERENCE

1. Tan Z, Chen S, Peng X, Zhang L, Gao C. Polyamide membranes with nanoscale Turing structures for water purification. *Science.* 2018;360(6388):518-521.
2. Kim JF, Kim JH, Lee YM, Drioli E. Thermally induced phase separation and electrospinning methods for emerging membrane applications: A review. *AIChE J.* 2016;62(2):461-490.
3. Yao Y, Zhang P, Jiang C, DuChanois RM, Zhang X, Elimelech M. High performance polyester reverse osmosis desalination membrane with chlorine resistance. *Nat Sustain.* 2021;4(2):138-146.
4. Nunes SP, Culfaz-Emecen PZ, Ramon GZ, et al. Thinking the future of membranes: Perspectives for advanced and new membrane materials and manufacturing processes. *J Membr Sci.* 2020;598:117761.
5. Wang Z, Deshmukh A, Du Y, Elimelech M. Minimal and zero liquid discharge with reverse osmosis using low-salt-rejection membranes. *Water Res.* 2020;170:115317.
6. Epsztein R, DuChanois RM, Ritt CL, Noy A, Elimelech M. Towards single-species selectivity of membranes with subnanometre pores. *Nat Nanotechnol.* 2020;15(6):426-436.
7. Cohen-Tanugi D, McGovern RK, Dave SH, Lienhard JH, Grossman JC. Quantifying the potential of ultra-permeable membranes for water desalination. *Energ Environ Sci.* 2014;7(3):1134-1141.
8. Echaide-Górriz C, Malankowska M, Téllez C, Coronas J. Nanofiltration thin-film composite membrane on either the internal or the external surface of a polysulfone hollow fiber. *AIChE J.* 2020;66(6):e16970.
9. Ritt CL, Werber JR, Wang M, et al. Ionization behavior of nanoporous polyamide membranes. *P Natl Acad Sci USA.* 2020;117(48):30191-30200.
10. Bhattacharjee S, Chen JC, Elimelech M. Coupled model of concentration polarization and pore transport in crossflow nanofiltration. *AIChE J.*

2001;47(12):2733-2745.

11. Epsztein R, Shaulsky E, Dizge N, Warsinger DM, Elimelech M. Role of Ionic Charge Density in Donnan Exclusion of Monovalent Anions by Nanofiltration. *Environ Sci Technol.* 2018;52(7):4108-4116.
12. Liang Y, Zhu Y, Liu C, et al. Polyamide nanofiltration membrane with highly uniform sub-nanometre pores for sub-1 Å precision separation. *Nat Commun.* 2020;11(1):2015.
13. Zhang F, Wu Y, Li W, Xing W, Wang Y. Depositing lignin on membrane surfaces for simultaneously upgraded reverse osmosis performances: An upscalable route. *AIChE J.* 2017;63(6):2221-2231.
14. Jaramillo H, Boo C, Hashmi SM, Elimelech M. Zwitterionic coating on thin-film composite membranes to delay gypsum scaling in reverse osmosis. *J Membr Sci.* 2021;618:118568.
15. Ruan X, Xu Y, Liao X, et al. Polyethyleneimine-grafted membranes for simultaneously adsorbing heavy metal ions and rejecting suspended particles in wastewater. *AIChE J.* 2017;63(10):4541-4548.
16. Gao S, Zhu Y, Gong Y, Wang Z, Fang W, Jin J. Ultrathin Polyamide Nanofiltration Membrane Fabricated on Brush-Painted Single-Walled Carbon Nanotube Network Support for Ion Sieving. *ACS nano.* 2019;13(5):5278-5290.
17. Karan S, Jiang Z, Livingston AG. MEMBRANE FILTRATION. Sub-10 nm polyamide nanofilms with ultrafast solvent transport for molecular separation. *Science.* 2015;348(6241):1347-1351.
18. Li S-L, Shan X, Zhao Y, Hu Y. Fabrication of a Novel Nanofiltration Membrane with Enhanced Performance via Interfacial Polymerization through the Incorporation of a New Zwitterionic Diamine Monomer. *ACS Appl Mater Inter.* 2019;11(45):42846-42855.
19. Yuan B, Li P, Wang P, et al. Novel aliphatic polyamide membrane with high mono-/divalent ion selectivity, excellent Ca2+, Mg2+ rejection, and improved antifouling properties. *Sep Purif Technol.* 2019;224:443-455.

20. Sarkar P, Modak S, Karan S. Ultraselective and Highly Permeable Polyamide Nanofilms for Ionic and Molecular Nanofiltration. *Adv Funct Mater.* 2021;31(3):2007054.
21. Wang Y, Liu L, Xue J, Hou J, Ding L, Wang H. Enhanced water flux through graphitic carbon nitride nanosheets membrane by incorporating polyacrylic acid. *AIChE J.* 2018;64(6):2181-2188.
22. Cao X-L, Guo J-L, Cai J, et al. The encouraging improvement of polyamide nanofiltration membrane by cucurbituril-based host–guest chemistry. *AIChE J.* 2020;66(4):e16879.
23. Di Vincenzo M, Tiraferri A, Musteata V-E, et al. Biomimetic artificial water channel membranes for enhanced desalination. *Nat Nanotechnol.* 2021;16(2):190-196.
24. Gong Y, Gao S, Tian Y, et al. Thin-film nanocomposite nanofiltration membrane with an ultrathin polyamide/UIO-66-NH2 active layer for high-performance desalination. *J Membr Sci.* 2020;600:117874.
25. Werber JR, Osuji CO, Elimelech M. Materials for next-generation desalination and water purification membranes. *Nat Rev Mater.* 2016;1:16018.
26. Shen L, Yi M, Japip S, et al. Breaking through permeability–selectivity trade-off of thin-film composite membranes assisted with crown ethers. *AIChE J.* 2020:e17173.
27. Werber JR, Deshmukh A, Elimelech M. The Critical Need for Increased Selectivity, Not Increased Water Permeability, for Desalination Membranes. *Environ Sci Tech Let.* 2016;3(4):112-120.
28. Liu TY, Yuan HG, Li Q, et al. Ion-Responsive Channels of Zwitterion-Carbon Nanotube Membrane for Rapid Water Permeation and Ultrahigh Mono-/Multivalent Ion Selectivity. *ACS nano.* 2015;9(7):e7488.
29. Kong X, Qiu Z-L, Lin C-E, et al. High permselectivity hyperbranched polyester/polyamide ultrathin films with nanoscale heterogeneity. *J Mater Chem A.* 2017;5(17):7876-7884.
30. Zhou X, Wang Z, Epsztein R, et al. Intrapore energy barriers govern ion

transport and selectivity of desalination membranes. *Sci Adv.* 2020;6(48):e9045.

31. Yuan B, Zhao S, Hu P, Cui J, Niu QJ. Asymmetric polyamide nanofilms with highly ordered nanovoids for water purification. *Nat Commun.* 2020;11(1):e6102.
32. He S, Jiang X, Li S, Ran F, Long J, Shao L. Intermediate thermal manipulation of polymers of intrinsic microporous (PIMs) membranes for gas separations. *AIChE J.* 2020;66(10):e16543.
33. Luo J, Wan Y. Effects of pH and salt on nanofiltration—a critical review. *J Membr Sci.* 2013;438:18-28.
34. Epsztein R, Cheng W, Shaulsky E, Dizge N, Elimelech M. Elucidating the mechanisms underlying the difference between chloride and nitrate rejection in nanofiltration. *J Membr Sci.* 2018;548:694-701.
35. Lin Y-L, Chiang P-C, Chang EE. Removal of small trihalomethane precursors from aqueous solution by nanofiltration. *J Hazard Mater.* 2007;146(1):20-29.
36. Bhattacharya S, Gubbins KE. Fast method for computing pore size distributions of model materials. *Langmuir.* 2006;22(18):7726-7731.
37. Jimenez-Solomon MF, Song Q, Jelfs KE, Munoz-Ibanez M, Livingston AG. Polymer nanofilms with enhanced microporosity by interfacial polymerization. *Nat Mater.* 2016;15(7):760-767.
38. Kiriukhin MY, Collins KD. Dynamic hydration numbers for biologically important ions. *Biophys Chem.* 2002;99(2):155-168.
39. Wang KY, Chung T-S. Fabrication of polybenzimidazole (PBI) nanofiltration hollow fiber membranes for removal of chromate. *J Membr Sci.* 2006;281(1):307-315.